An In-situ FTIR Study of Ethanol Oxidation at Polycrystalline Platinum in 0.1M KOH at 25 °C and 50 °C.

*P. A. Christensen**[≠] *and S. W. M. Jones*[≠]

School of Chemical Engineering and Advanced Materials, Bedson Building, Newcastle University, Newcastle upon Tyne, NE1 7RU, England, UK.

Abstract

The electrochemical oxidation of ethanol at a polycrystalline Pt electrode was studied using in-situ Fourier Transform InfraRed (FTIR) spectroscopy in 0.1M KOH at 25 °C and 50 °C. It was found that the equilibrium between Pt and reversibly-adsorbed OH shifts to favour the latter at 50 °C compared to 25 °C, and this was reflected in the higher oxidation currents observed in the voltammetry, as well as increased production of acetate in the FTIR spectra. Acetate is the only product observed at lower potentials. Above the transition potential, where at least some of the areas of the thin layer in the spectro-electrochemical cell become acidic, acetaldehyde, acetic acid and a small amount of CO_2 are produced. This transition potential depends strongly on temperature: -0.1V at 25 °C and -0.4V at 50 °C. The temperature dependence of the production of acetaldehyde and acetic acid strongly suggests that the rate determining step is the removal of the first proton from the initially-adsorbed ethoxide species, and we tentatively suggest that this

is also the rds under alkaline conditions. Overall, our data provide additional support for the mechanism we have developed over a number of publications concerning the oxidation of small alcohols at polycrystalline Pt in alkaline electrolyte.

Keywords: Electrocatalysis, KOH, thin-layer, ethoxy, infrared spectroscopy, temperature

Introduction

Ethanol is generally perceived as a sustainable and "green" fuel as it can be produced in industrial quantities from the fermentation of sugar-containing crops or waste from agriculture[1], and it, and its complete oxidation product, CO_2 are relatively non-toxic. Furthermore, ethanol has a relatively high energy density, ca. 8 kWh kg^{-1}[2] and can be handled, transported and stored using the existing liquid fuel infrastructure. As a consequence, ethanol has been the focus of intense research with respect to its possible application as a fuel for fuel cells [3]. However, the high energy density of ethanol is only achieved if complete oxidation of the molecule is effected, and this has proved extremely problematic and the current efficiency for CO_2 remains low[1][4].

In recent years, attention has turned increasingly to alkaline fuel cells: noble metal catalysts under alkaline conditions exhibit lower overpotentials towards the oxidation of small organic molecules (and oxygen reduction); further, a wider range of materials are stable in alkaline electrolyte and are catalytically active. Thus, alkaline fuel cells using aqueous electrolyte are the best performing of all known fuel cells[5][6] and have been exploited since the early 1960's[7].

However, problems associated with the aqueous KOH employed, (including high wetting ability and hence tendency to cause leaks, and carbonation of the electrolyte), restricted their application largely to space exploration[5], and precluded the use of air as oxidant or organic molecules as fuel. Recent developments have radically changed the field of alkaline fuel cells, centred on the development of alkaline analogues of polymer electrolyte membranes such as Nafion (Alkaline Anion Exchange Membranes, or AAEM's see, for example, [8][9] and references therein) in which it has been postulated that carbonation should not be a problem.

Rao et al.[10] reported data on an AAEM-based Membrane Electrode Assembly with hydrogen fed to the cathode (which also acted as a reference electrode) in which ethanol was oxidised at 0.8V *vs* the cathode (ie vs the RHE; the system operating as an electrolysis cell) and the products monitored using Differential Electrochemical Mass Spectrometry (DEMS). The anode and cathode were unsupported Pt black, the loading of the latter was 4 mg cm^{-2}, the loading of the former was not specified. The authors observed a current efficiency for CO_2 formation of 55%, compared to only 2% when using (an unspecified) acidic PEM. Thus it appears that alkaline fuel cells offer the possibility of significant current efficiency for CO_2 production in addition to their other advantages, although this has not been supported by fundamental studies, see discussion below.

Whilst there are fundamental studies on ethanol oxidation at Pt and Pt-based catalysts in alkaline solution, the literature in this area suffers from a lack of analytical/molecular information. The mechanism of ethanol oxidation at Pt is usually assumed to be the same as in acid, ie. the Dual Path mechanism, see scheme 1:

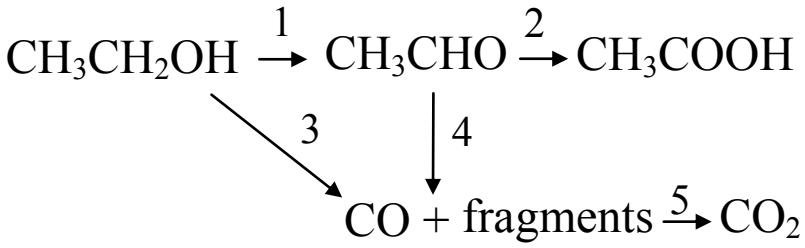

Scheme 1. The Dual Path mechanism.

There are far fewer studies on ethanol oxidation under alkaline conditions than in acid. In the latter, the presence of adsorbed CO, CO_{ads}, is taken as evidence for the "indirect path" (steps 1, 3, 5 and/or 1, 4, 5 in Scheme 1), resulting in bond cleavage and CO_2 formation. The "direct path" (steps 1 and 2) produces acetic acid and acetaldehyde, both of which are stable with respect to further oxidation due, it is generally believed, to the blocking of the Pt surface by some of the chemisorbed fragments[11][12]; Shao and Adzic[11] suggest that the blocking of active sites is due to adsorbed acetate. In addition, the intermediates in the formation of acetaldehyde and acetic acid remain unclear[13 – 15]. Hence, while there is general agreement around the broad principles encapsulated by scheme 1, the exact details of the mechanism whereby solution ethanol is oxidized to acetic acid, acetaldehyde, and small amounts of CO_2 remains controversial[1][16].

Reports on ethanol oxidation in alkaline electrolyte generally infer the existence of some form of adsorbed CO (CO_{ads}) [17] without any direct, molecular evidence for its formation. For example, Jiang et al[18] observed two peaks in the forward sweep of cyclic voltammograms of

carbon-supported Pt particles in aqueous NaOH/ethanol. By comparison to the case in acid solution[19], the peak at lower potential was assigned primarily to the complete oxidation of ethanol, and the second to its partial oxidation to acetate ions. As carbonate was a product, then it followed that CO_{ads} was the intermediate. Similarly, López-Atalaya et al[20] attribute stripping peaks in the voltammogram of ethanol chemisorbed on single-crystal Pt surfaces to the oxidation of CO_{ads} as the peaks were the same as observed when CO gas was adsorbed onto the electrodes.

Overall, under alkaline conditions, there is a heavy reliance on voltammetry to provide evidence for the dual path mechanism, despite the inability of the technique to provide molecular information. Further, there is some confusion with respect to the interpretation of the hysteresis generally observed in cyclic voltammogramms of Pt in ethanolic hydroxide solutions between the forward and reverse sweeps. Thus, Dutta and Datta[17] employ the ratio of the ethanol oxidation peak currents in the forward and back (reverse) sweeps, I_F/I_B, as a measure of the efficacy of the stripping of the Pt oxide at removing adsorbed, carbonaceous fragments. The higher this ratio, the more effective the oxidation of adsorbed species. In an earlier paper[2], they postulated that the formation of surface oxides activated the Pt surface to the oxidation of adsorbed species. However, in general, it is accepted that oxidation of adsorbed ethanol in alkali electrolyte takes place at lower potentials via reversibly-adsorbed OH_{ads}, and the oxidation of the Pt to Pt-OH or Pt-O inhibits ethanol oxidation at higher potentials[18][21]. The higher I_F/I_B, the more effective OH_{ads} is at oxidising adsorbed species. The extent of the hysteresis between the forward and reverse scans in a cyclic voltammogram at potentials ≤ that of the anodic peak in the reverse scan is also taken as an indication of the coverage by strongly adsorbed

species[1][13][21]; the greater the hysteresis, the greater the influence of adsorbed species (such as CO_{ads}).

A further example of the pitfalls of relying upon techniques incapable of providing molecular information to provide analytical data is provided by the work of Caram and Guitiérrez[22]. The authors employed polarization modulation reflectance spectroscopy (PMRS) to study methanol and ethanol chemisorption in acid and alkaline electrolyte at a polycrystalline Pt electrode. A peak at 270 nm was observed for methanol and ethanol in 0.5M $HClO_4$, and was attributed to linearly-adsorbed C≡O (CO_L). The same feature was observed for methanol chemisorption in 1M NaOH, but not observed in the PMRS spectrum of ethanol in 1M NaOH, despite the amount of adsorbed CO, as estimated from cyclic voltammetry via oxidative stripping, being the same as observed with methanol under the same conditions. The authors could not explain the absence of the CO_L peak. It does not seem unreasonable to suppose that the stripping peak from ethanol chemisorption in NaOH was (primarily) due to adsorbed species other than CO_L.

There are papers reporting molecular data to support the indirect path. Thus, Dutta and Datta[17] analysed the products from 1M ethanol oxidation in 0.5M NaOH at carbon-supported Pt particles using ion exchange chromatography (IEC). The authors' IEC data appeared to show carbonate production favoured over acetate at all the temperatures studied, 20 – 80 ºC, and increasing with increasing temperature. However, the ordinate axes on the relevant plots were unlabelled in terms of units, and no attempt appeared to have been made to render the IEC data quantitative. Lai et al[1] present Surface Enhanced Raman (SER) spectra collected from a Pt electrode covered with chemisorbed ethanol in the absence of ethanol in solution. Bands were

observed at 440 and 515 cm^{-1}, attributed to two different forms of linearly adsorbed CO, and at 1960 and 2035 cm^{-1} attributed to bridge-bonded and linearly adsorbed CO, respectively. These were taken as evidence for the presence of adsorbed CO in the voltammetric experiments using single crystal Pt electrodes. However, it is not clear that the SERS electrode, consisting of electrochemically roughened gold on which Pt was electrodeposited a few monolayers thick, is representative of bulk Pt. The authors maintained that the thickness of the platinum layer was high enough to mask the electrochemical properties of the gold layer beneath. In contrast, in our studies of metallic multilayer nanostructured catalysts, we have found that overlying layers even hundreds of monolayers thick are unable to mask the influence of the underlying layers[23][24]. Further, a correlation between the SERS band intensities and, for example, the observed Faradaic current, was not attempted. In a later paper, the same workers present a comprehensive study of ethanol electro-oxidation at polycrystalline gold and platinum electrodes as a function of pH using cyclic voltammetry, in-situ external reflectance FTIR spectroscopy, and SERS. Unfortunately, as discussed in detail in our previous paper[25] the (key) alkaline FTIR data is highly suspect, possibly due to an abnormally thin layer between the electrode and cell window, leading to an immediate pH drop to acidic values as soon as Faradaic current passed. Lopéz-Atalaya et al[20] employed Subtractively Normalised Interfacial Fourier Transform Infrared spectroscopy (SNIFTIRS)[26][27] and conventional in-situ FTIR spectroscopy to study ethanol electro-oxidation at Pt(111), Pt(110) and Pt(100) electrodes in aqueous NaOH and Na_2CO_3. Whilst the authors did observe weak features due to linearly adsorbed and multiply-bonded CO_a, the only product observed using all three electrodes was acetate. They concluded that adsorbed CO was responsible for poisoning the Pt(111) electrode (the other electrodes deactivated primarily due to structural modifications), but did not attempt to elucidate the mechanism of

ethanol oxidation. The conclusions of Lopéz-Atalaya and co-workers are in direct contrast to the theory of Lai and Koper[36] based on the latter's studies of ethanol oxidation at single crystal Pt electrodes in 0.1M NaOH. Lai and Koper postulate that adsorbed CO is the only strongly adsorbed intermediate at co-ordinately unsaturated surfaces such as Pt(110), whilst CH_x is responsible for poisoning surfaces with long terraces, such as Pt(111).

Overall, we are not convinced by the evidence in favour of adsorbed CO as a key intermediate in the oxidation of ethanol in aqueous alkaline electrolyte, or that chemisorption of ethanol at Pt under such conditions takes places via cleavage of C-H bonds. In our earlier paper [25], we have proposed the mechanism shown in scheme 2 for ethanol oxidation at polycrystalline Pt in aqueous KOH. Thus, initial adsorption of ethanol gives the adsorbed ethoxy intermediate (I). Oxidation of this by adsorbed OH [28] generates (II) and further oxidation by OH_{ads} yields monodentate acetate (III). The presence of ethanol in solution and hence ethanol adsorption replaces (II) at the surface, releasing acetaldehyde; similarly, displacement of (III) releases acetate, which is the predominant product. Under conditions of ethanol starvation, the bidentate adsorbate (IV) is formed which can undergo further oxidation to give carbonate. The bands attributed to (I) to (IV) are summarized in table 1.

The work reported in this paper is an extension of our previous studies, by considering the effect of temperature on ethanol oxidation at polycrystalline Pt in 0.1M KOH.

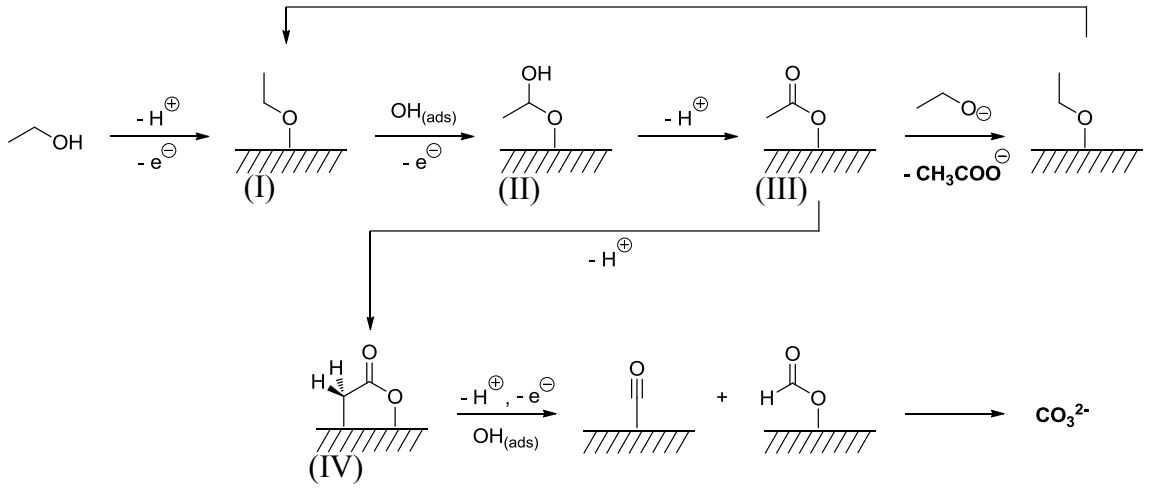

Scheme 2. The mechanism of ethanol oxidation at polycrystalline Pt in alkaline solution [25].

Experimental

The electrolyte solutions were prepared using Millipore water (18.2 MΩ cm). Aqueous 0.1 M KOH (Aldrich SigmaUltra >85% KOH basis) was employed as supporting electrolyte. In order to ameliorate pH effects in the thin layer (see below) it would have been advantageous to employ higher concentrations of KOH, but such concentrations would lead to an unacceptably high rate of etching of the prismatic window. Ethanol (Aldrich spectrophotometric grade >99.9% ACS) was used as received. Nitrogen gas from a cryogenic boil-off was employed to de-aerate the solutions and to maintain an air-free atmosphere over the electrolyte during the measurements. All potentials are given *vs*. the Hg/HgO (Mercury Mercury Oxide, MMO Sentek) electrode in aqueous 0.1M NaOH. The polycrystalline Pt electrode was 'top hat' shaped with an area of 0.64 cm^2 polished and exposed to the electrolyte [29][30].

The electrode was polished with 0.015 μm alumina (BDH), washed thoroughly with Millipore water and then immersed in Millipore water in an ultrasonic bath for several minutes prior to transfer into the spectro-electrochemical cell. The cleanliness of the electrolyte and cell were assessed by cyclic voltammetry.

The spectroelectrochemical cell has been described in detail elsewhere [30] and employed a hemispherical cell window. The IR beam was unpolarised. The cell was mounted vertically on the lid of the sample compartment of the spectrometer via an aluminium plate, and was designed to allow electrolyte exchange under potential control. The cell was fitted with a heating/cooling jacket, thus allowing for control of the electrolyte temperature within the cell, using a Grant GD120 R1 water bath. Insulated pipes running from the water bath were passed through the cell jacket and hollow cell base, allowing water to flow and maintain the required electrolyte temperature in the bulk of the cell and thin layer.

The *in-situ* FTIR experiments were carried out as follows: after collecting a cyclic voltammogram in the absence of ethanol to check for cleanliness, the potential was held at -0.85V and ethanol added to a final concentration of 1 M, after which the electrode was pressed against the CaF_2 cell window and the spectrometer allowed to purge free of CO_2 and water vapour (*ca*. 30 - 60 minutes). The reference spectrum (S_R, 100 co-added and averaged scans at 8 cm^{-1} resolution, *ca*. 35 s per scanset) was collected and a second spectrum taken at the same potential (to check for electrode movement *etc*), after which spectra (S_S) were collected at -0.8V and then every 100 mV up to 0.4V *vs* MMO. The spectra below are presented as:

Absorbance, $A = Log_{10}(S_S/S_R)$ (1)

This data manipulation results in difference spectra in which peaks pointing up, to +(Absorbance), arise from the gain of absorbing species in S_S with respect to S_R, and peaks pointing down, to -(Absorbance), to the loss of absorbing species. Spectra obtained at higher potentials were normalised by subtraction, eg $A_{0.4V} - A_{0V}$, see below.

The optical pathlength was estimated from the 1640 cm^{-1} H-O-H scissor band in the single beam reference spectrum, as described elsewhere[29 - 32], and this was employed to ensure consistent thin layer thicknesses of *ca*. 1.0 μm. In order to ensure appropriate and reproducible alignment between experiments the intensities at 2500 cm^{-1} and 1900 cm^{-1} in the single beam spectra were employed[33]. The maximum throughput at 1900 cm^{-1} was found to be ca. 12 – 14 V with a thin layer thickness of ca. 1 μm, and the contact between the reflective working electrode and CaF_2 prism was adjusted until a value of I_2 in this range was obtained. The ratio I_2/I_1 was then taken as an indication of the alignment of the spectrometer (as poor mirror alignment results in the loss of energy across the mid-IR, with the greatest effect at frequencies > 1500 cm^{-1}[34]), and good alignment was defined as $I_2/I_1 > 0.75$.

Analytical cyclic voltammetry experiments (as opposed to those carried out in the spectro-electrochemical cell to check system cleanliness) were carried out in a standard, 3-electrode glass cell comprising a 1 cm^2 Pt foil working electrode co-facial with a 6 cm^2 Pt/Ti mesh counter electrode (50% open area), and a Mercury Mercury Oxide (MMO, Sentek) reference electrode.

In both the cyclic voltammetry and *in-situ* FTIR experiments, the electrolytes were sparged with N_2 gas prior to data collection. During data collection, a blanket of N_2 was maintained above the electrolyte without sparging through the solution.

Results and Discussion

Cyclic voltammetry

Figure 1 shows cyclic voltammograms of a Pt (foil, 1cm x 1cm) electrode immersed in 0.1 M KOH in the absence of ethanol at 25 and 50 ^{o}C. From the figure, it may be seen that features corresponding to the formation of reversibly-adsorbed OH (OH_{ads}, peak near -0.19V)[18][21] and the formation and stripping of chemisorbed hydride and oxide layers on the Pt surface[35] were observed. The charge under the OH_{ads} peak in the anodic scan is higher at 50 ^{o}C than at 25 ^{o}C suggesting that the equilibrium:

$$Pt + OH^- \leftrightarrow PtOH + e^- \quad (2)$$

shifts to the right at the higher temperature, in agreement with the postulate by Datta and co-workers [2][17] that OH_{ads} formation is more facile at higher temperature in alkaline solution, and hence ethanol oxidation faster. Figure 1 also shows that the maximum of the peak due to reduction of the phase oxide, formed at Pt during the anodic sweep of the CV, shifts from ca. -0.16 to -0.10 V upon increasing the temperature from 25 to 50^{o}C.

Figure 2 shows the corresponding cyclic voltammogramms collected in the presence of 1M ethanol. As can be seen from the figure, the hydrogen adsorption region is blocked by

chemisorbed fragments of ethanol[18][21][36], and the oxidation of ethanol commences with OH_{ads} formation[21]. Both anodic peaks in the forward and reverse sweeps of the CV in fig. 2 increase in current with temperature, in contrast to Ma *et al* [21] who have reported a decrease in current density during the forward scan upon increasing the temperature from 40 to 60^{o}C. The authors attributed this to an increase in carbonate formation, indicated by an additional peak at ca. 0.5 V vs. RHE in the CV. Datta and co-workers [2][17] have also suggested that the ratio of carbonate to acetate formation increases with increasing temperature. It is difficult to discern from fig. 2 whether the anodic peak in the forward scan of the voltammogram is comprised of two waves, as per the work of Jiang et al[18] and Ma and colleagues[21]. In the absence of molecular information, the possible production of carbonate cannot be resolved, hence the in-situ FTIR studies reported below.

There appears to be no difference in onset potential for ethanol oxidation in the forward sweep, in agreement with Jiang et al[18] and Ma and co-workers[21]; the latter reported that the onset potential depended on the ethanol concentration. However, it is clear that the peak in the forward sweep moves to higher potentials with increasing temperature; from -0.13V at 25ºC to -0.08V at 50ºC.

As may be seen from fig. 2, at all temperatures, the oxidation of ethanol during the forward sweep was suppressed due to the oxidation of the Pt to Pt-OH or Pt-O[18][36]. The potential at which the current falls to ca. 5% of its value at the anodic peak in the forward scan was +0.14V and +0.17V as the temperature was increased from 25 to 50ºC. From fig. 1, it can be seen that the onset of formation of the Pt-OH does not seem to vary with temperature, although the

coverage of the oxide/hydroxide layer (ie. at potentials > -0.1V) is significantly higher at 50ºC than at the lower temperatures, suggesting that the higher temperature facilitates oxidation of ethanol at the oxidised Pt, as is observed in acid solution[1].

In the reverse sweep in fig. 2, the increasing anodic potential of the onset of ethanol oxidation peak appears to follow the temperature dependence of the oxide stripping peak, see fig. 1. The data in fig. 2 at 50ºC resemble the CV's reported by Lai et al[36] for polycrystalline Pt in 0.1M NaOH+0.5M ethanol at room temperature, in that there is very little hysteresis between the forward and reverse scans at potentials below the anodic peak in the reverse scan, ie. -0.18V vs MMO, suggesting that the steady state coverage of the Pt by carbonaceous fragments is achieved more rapidly at 50 °C compared to 25 °C .

In-situ FTIR data at potentials below transition

As described in our previous papers[25][31][32], at higher potentials during our *in-situ* FTIR experiments in alkaline solution there is a substantial change in pH in the electrolyte immediately above the electrode and trapped in the thin layer. This corresponds to a transition in behaviour from alkaline to acid electrocatalysis; the potential at which this transition occurs (the transition potential) depends upon the temperature (see below). The swing in pH at higher potentials was ascribed to a combination of [31][32]: (a) relatively slow diffusion of OH^- ions across the electrode surface over a timescale of tens of minutes for an electrode of the radius that we use; and (b) the exhaustion of reactant in the thin electrolyte layer, which leads to further changes in the ambient conditions at the electrode surface. Thus, the data presented in this section will be

discussed in two sections, ie. the spectra collected (1) below and (2) above the transition potentials of -0.1V (25 ºC) and -0.4V (50 ºC).

Figure 3 shows the spectra collected during an experiment carried out at 50 °C in 0.1 M KOH + 1 M ethanol. The potential was stepped from -0.85 V to +0.4 V vs MMO, but the figure shows only the spectra collected up to the transition potential of -0.4 V. At 25 °C, this transition occurred at -0.1 V. The spectra in fig. 3 are representative of the data observed at both temperatures, in that the only features observed were due to solution acetate and hydroxide ions, and water. As may be seen from the figure, the spectra are dominated by broad loss features with minima near 1870 and 2750 cm^{-1},and gain features at 1554, 1415 and 1348 cm^{-1}. The gain features may be unambiguously assigned to solution acetate[25][37][38]. By a diffusion experiment, the gain features have been attributed to solution hydroxide ions [39]. This assignment is confirmed by the work of Śmiechowski and Stanget [40] (compare figs. 3(a) and (b)).

In agreement with López-Atalaya et al[20] and in contrast to the postulated carbonate formation in the various papers reporting IVt data on ethanol oxidation at Pt/C in alkaline solution[2][17][18][21], there is no evidence for CO_3^{2-} in fig. 3.

Figure 4 shows the spectra collected at the transition potentials of -0.1V (25 °C) and -0.4V (50 °C) normalized to the respective reference spectra collected at -0.85V. As can be seen from the figure, the intensities of the acetate features are comparable, despite the 50 °C spectrum having been taken at a potential 300 mV lower than that collected at 25 °C. There is also a difference in

terms of the behaviour of the water features (see below). These may be clearly seen in figs. 5(a) and (b) which show plots of the intensities of the various key features in the spectra collected during the experiments depicted in fig. 3 as a function of potential (the spectra employed to determine these intensities were all normalized to -0.85V); the arrows in fig. 5(b) mark the transition potentials above which CO_2 and acetic acid were observed. Figure 5(b) shows the plots in fig. 5(a) normalised to their maximum values to highlight concomitant behaviour.

Figure 6 shows the spectra collected at -0.6 V vs. MMO in the experiments at 25 and 50^{o}C. As may be seen from the figure, the intensity of the sharp gain feature at ca. 3670 cm^{-1}, which may be attributed to isolated OH (ie Pt-O-H free from hydrogen bonding [41][42]), is significantly greater at 50^{o}C than at 25^{o}C; if this is OH_{ads}, then the data in fig. 6 are in agreement with the voltammetry data in figs. 1 and 2 showing enhanced current for OH_a formation at 50°C .

The spectra in figs. 3 and 4 are dominated by the solution OH^- loss feature [25][31][32] with peaks near 2750 cm^{-1} and 1870 cm^{-1} due to its reaction with adsorbed ethanol species to form acetate. The intensities of these features increase more rapidly with potential in the spectra collected at 50 ^{o}C than at 25 ^{o}C, see figs 5(a) and (b). As can be seen from fig. 5(b), at both temperatures, the 1870 cm^{-1} OH^- loss and 1415 cm^{-1} acetate gain features track each other, reflecting the role of the former as a reactant in the oxidation of ethanol:

$$C_2H_5OH + 5\ OH^- \rightarrow CH_3COO^- + 4H_2O + 4e^- \quad (3)$$

It is also clear from figs. 5(a) and (b) that the intensities of the water O-H stretch features do not track the acetate bands, lagging some 300 mV behind at each temperature (and the water features at 50 °C appear as losses); this suggests that the processes responsible for the change in water absorptions are associated with events taking place at higher potentials. It appears that the slopes of the two plots in fig. 5 both increase at potentials above transition. From fig. 5(b) it can be seen that the onset potential for acetate production ($\geq$ -0.6V) corresponds that for the formation of adsorbed OH [25][28][31][32], which then oxidizes the adsorbed ethoxy species to acetate. Above the transition potentials, the acetate bands cease growing and are replaced by the gain features due to acetic acid[25]. From fig. 5(a) it is clear that there is a significant increase in acetate formation at all potentials below transition at 50 °C compared to 25 °C. This marked difference in behavior between the IR response at 50 °C on the one hand, and 25 °C on the other is reflected in the behavior of the O-H stretches near 3300 cm^{-1}. At 25°C, there is a steady, gain of an O-H stretch feature due to water at 3250 cm^{-1} and an attendant, weaker band near 1635 cm^{-1} due to the H-O-H deformation. In contrast, at 50°C, both the O-H stretch and H-O-H deformation appear as loss features, growing steadily in intensity as the potential is increased. We have no explanation for this behaviour at this time.

From fig. 3 it may be seen that the valley between the 1554 and 1415 cm^{-1} acetate absorptions is structured (arrowed) and, in addition, was shown in our previous work [25] to be deeper than that in the spectrum of aqueous sodium acetate. This was attributed to the loss of absorptions in this spectral region, even at potentials as low as -0.7V (at 25 °C), and these losses are described in the next section.

In-situ FTIR data at potentials above transition

Figures 7(a) and (b) show spectra collected at potentials > -0.3V in the experiment at 50 ºC normalised to that taken at -0.3V. These data were chosen as representative of both temperatures because the various features were observed in both experiments. In addition, the extended potential range possible at the higher temperature (lower transition potential) gave more data points for analysis, and the very weak intensity (or absence of) the 1554 cm^{-1} acetate band facilitated a more accurate determination of the intensities of the 1573 cm^{-1} and 1540 cm^{-1} bands[25].

As can be seen from fig. 7(a), there are sharp loss features at 2956, 2913 and 2850 cm^{-1}, the latter two of which appear to be bipolar. These bands may be attributed to adsorbed ethoxy species ([25] and references therein).

The gain of CO_2 (band at 2340 cm^{-1}) clearly shows that the pH, at least in some regions of the thin layer, has fallen below the pK_a of carbonic acid, 6.4 [25][31][32]. The gain features at 1715 cm^{-1}, 1378 cm^{-1} and 1280 cm^{-1} may be attributed to acetic acid, but with a contribution to the 1715 cm^{-1} band from acetaldehyde [25], see below. The formation of acetic acid clearly shows that the pH in the thin layer at these potentials is $\leq$ 4.7, the pK_a of acetic acid[43]; this value varies very little between 14 ºC and 45 ºC [44]. The substantial drop in pH in thin-layer FTIR spectroscopic experiments has been modelled in terms of the slow diffusion of OH^- ions across the electrode surface coupled with the exhaustion of reactant[31][32].

Figure 8 shows the spectra collected at 0.4V vs. MMO normalised to the transition potentials of -0.1 and -0.4 V during the ethanol oxidation experiments carried out at 25 and 50 ^{o}C respectively. As may be seen from figs 7(a) and 8, intense loss features near 3600, 3400 and 1650 cm^{-1} appear and grow after the transition point during the experiment carried out at 50 ^{o}C. In order to determine whether the water loss features observed at 50 °C were associated with the oxidation of ethanol at this temperature, spectra were collected during experiments analogous to those depicted in fig. 3 but in the absence of 1 M ethanol, and the results are shown in fig. 9.

Comparing figs. 8 and 9 shows that the water gain features above 2750 cm^{-1} and at ca. 1640 cm^{-1} observed during the oxidation of ethanol at 25 ºC and potentials above -0.1V are also observed in the absence of ethanol. In contrast, there is a clear and marked change in behaviour of the water features at 50 ºC in the absence of ethanol compared to in the presence, with the gain of various water-related bands in the absence of ethanol being replaced by a significant loss, potentially showing a change in mechanism, in contrast to the work of Datta and co-workers [2][17] and Ma et al[21]. However, similar water loss features were observed in our previous studies on methanol oxidation in KOH[31] and attributed to the loss of highly hydrogen-bonded bulk water[45] from the thin layer due to CO_2 gas bubble formation, and this does not seem an unreasonable explanation, particularly given the fact that the other loss features (see table 1) and gain features are observed at both temperatures, suggesting a single mechanism.

Taking the gain features in figs. 7 and 8 first, fig. 10 shows the spectra depicted in fig. 8 over the range 2050 – 1050 cm^{-1}. As was stated above, the gain features at 1715 cm^{-1}, 1378 cm^{-1} and 1280 cm^{-1} may be attributed to acetic acid[25]. However, the ratio of the band intensity at 1715

cm^{-1} to that at 1280 cm^{-1} is significantly greater in the spectrum collected at 50 ^{o}C, indicating a contribution to the 1715 cm^{-1} band from (an)other species. It is generally accepted that the carbonyl stretch of acetaldehyde occurs in the same spectral region as the 1715 cm^{-1} carbonyl stretch of acetic acid [13][16], rendering any quantitative assessment of these compounds using these absorptions highly challenging. However, the 1280 cm^{-1} band of acetic acid is not obscured by any absorptions due to the aldehyde and is the same intensity as the carbonyl feature at 1715 cm^{-1}[25]; hence the difference between the intensities of the 1715 cm^{-1} and 1280 cm^{-1} bands in fig. 10 may be taken as a (crude) estimation of the acetaldehyde carbonyl absorption. Close inspection of all the experiments carried out reveals a trend in that the greater the difference between the 1712 cm^{-1} and 1280 cm^{-1} bands, ie. the more acetaldehyde produced, the more pronounced is the bipolar nature of the C-H bands, suggesting that acetaldehyde formation is actually responsible for the bipolar nature of these bands.

Figure 11 shows plots of the intensities of the various features in figs. 7(a) and (b) as a function of potential. As can be seen, the amount of acetic acid in the thin layer increases steadily with increasing potential, whilst the acetaldehyde reaches a maximum value at ca. 0.3V. The CO_2 increases relatively slowly as the potential is increased. The intensities of the acetaldehyde C=O band (calculated from the difference in intensities of the 1280 and 1715 cm^{-1} absorptions) and the 1280 cm^{-1} feature of acetic acid at 0.4V are presented in table 2; as can be seen the ratio of the former to the latter at both temperatures is ca. 1.4:1, with ca. twice as much acetaldehyde and acetic acid produced at 50 °C as at 25 °C. Hence both acetaldehyde and acetic acid are produced faster at the higher temperature, but this increase is the same, maintaining the ratio of the products. This is a crucial result as it strongly suggests that the rate-determining step

in the oxidation of ethanol under the acidic conditions in fig. 11 is the removal of the first proton from the adsorbed ethoxy species (I), and that the desorption of acetaldehyde and the further oxidation of species (II) to acetate must take place at comparable rates and with similarly low activation energies. It does not seem unreasonable to postulate that this first removal of hydrogen is also the rate determining step in alkaline electrolyte.

Returning to the loss features in figs. 7, 8 and 10, it may be seen that the loss feature at ca. 1540 cm^{-1}, which is attributed to the C=O stretch of bidentate carbonate (see table 1), was significantly more intense in the spectra collected at 50 ºC than at 25 ºC. Thus this suggests that C-C bond scission is enhanced at higher temperature under alkaline conditions. However, the intensity of this feature is very low when compared to the acetate features observed before the transition point and there is no obvious solution carbonate band in the spectra in figs 7 or 10, suggesting that even at 50 ^{o}C, complete oxidation of EtOH to carbonate has only a minor contribution to the overall oxidation process.

The 1573 cm^{-1} band was assigned in our previous work[25] to the C=O stretch of acetate adsorbed through one O atom (Pt_s-O-C(=O)CH_3)), and the 1475 cm^{-1} feature to the C-H deformation of the same species [25]; both bands were more intense in the spectra collected at 50 ^{o}C compared to those at 25 ºC. In addition, the loss features at ca. 2956, 2915 and 2850 cm^{-1}, previously assigned to adsorbed ethoxy [25], are of much greater intensity in the spectra collected at 50 ^{o}C than those collected at 25 ^{o}C. Hence, it is clear that increasing the temperature to 50 ^{o}C significantly enhances ethanol adsorption (as Pt-O-C_2H_5) at Pt at low potentials, and its subsequent oxidation to produce acetaldehyde and acetate.

Conclusions

The surface of the polycrystalline Pt electrode is extensively covered with adsorbed ethoxy at both 25 and 50 ^{o}C even at low potentials in aqueous KOH, with the (non-dissociatve) chemisorption of ethanol enhanced upon increasing the temperature. Oxidation of the ethoxy species results in acetate, which is the predominant product under conditions of ethanol excess in solution. The oxidation of adsorbed ethanol to form acetate at lower potentials ($\leq$ -0.1V at 25 ºC and $\leq$ -0.4V at 50 ºC) is enhanced significantly upon heating from 25 ºC to 50 ^{o}C, which is associated with the increased coverage of OH_{ads}.

In contrast to some reports in the literature, there is no evidence of carbonate production in the spectra collected below the transition potentials at 25 or 50 ºC. Small quantities of carbon dioxide are produced at potentials above transition, where the electrolyte in the thin layer is acidic, and acetic acid and acetaldehyde are also produced; the temperature dependence of this process strongly suggesting that the rate determining step in the oxidation is the removal of the first hydrogen atom from adsorbed ethoxide.

Tables

Band /cm-1	**Assignment**
2985, 2913, 2846	C-H stretches of adsorbed ethoxy (I)
1573	ν_s adsorbed unidentate acetate, Pt_s-O-C(=O)CH_3 (III)
1475	C-H deformation of adsorbed unidentate acetate, Pt_s-O-C(=O)CH_3 (III)
1554	ν_{as} solution acetate
1415/1418	ν_s solution acetate
1540	Uncoordinated C=O stretch of bidentate adsorbed carbonate or C=O stretch of Pt_s-CH_2COOPt (IV)
1274	Pt_s-CH(OH)CH_3 (II)

Table 1. The assignment of the various features attributed to adsorbed C and O containing species, and bands due to solution acetate. See text for details[20].

Temperature /°C	**$C=O_{Acid}$ /10^{-3}**	**$C=O_{Ald}$ /10^{-3}**
25	2.0	2.7
50	4.0	5.8

Table 2. The intensities of the acetic acid ($C=O_{Acid}$) and acetaldehyde ($C=O_{Ald}$) absorptions in figs. 7(a) and (b), see text for details.

Corresponding Author

Prof. Paul A. CHRISTENSEN

School of Chemical Engineering and Advanced Materials, Bedson Building, Newcastle University, Newcastle upon Tyne, NE1 7RU, UK

Tel: +44(0) 191 222 5472

paul.christensen@ncl.ac.uk

Author Contributions

The manuscript was written through contributions of all authors. All authors have given approval to the final version of the manuscript. ≠

Acknowledgement

We should like to thank the EPSRC for funding under the Hydrogen and Fuel Cells Supergen initiative and Dr. A. Hamnett for helpful discussions.

References

1. Lai, S. C. S.; Kleijn, S. E. F.; Öztürk, F. T.; van Rees Vellinga, V. C.; Koning, J.; Rodriguez, P.; Koper, M. T. M., Effects of electrolyte pH and composition on the ethanol electro-oxidation reaction. Catal. Today. 2010, 154, 82-104.

2. Mahapatra, S. S.; Dutta, A.; Datta, J., Temperature effects on the electrode kinetics of ethanol oxidation on Pd modified Pt electrodes and the estimation of intermediates formed in alkali solution. Electrochim. Acta. 2010, 55, 9097-9104.

3. Kamarudin, M. Z. F.; Kamarudin, S. K.; Masdar, M. S.; Daud, W. R. W., Review: Direct ethanol fuel cells. Int. J. Hydrogen Energy. 2013, 38(12), 9438-9453

4. Friedl, J.; Stimming, U., Model catalyst studies on hydrogen and ethanol oxidation for fuel cells. Electrochim. Acta. 2013, 101, 41-58.

5. Varcoe, J. R.; Slade, R. C. T., Prospects for alkali anion-exchange membranes in low temperature fuel cells. Fuel Cells. 2005, 5, 187-200.

6. McLean, G. F.; Niet, T.; Prince-Richard, S.; Djilali, N., An assessment of alkaline fuel cell technology. Int. J. Hydrogen Energy. 2002, 27, 507-526.

7. Lin, B. Y. S.; Kirk, D. W.; Thorpe, S. J., Performance of alkaline fuel cells: A possible future energy system?, J. Power Sources. 2006, 161, 474-483.

8. Luo, Y.; Guo, J.; Wang, C.; Chu, D., Fuel cell durability enhancement by crosslinking alkaline anion exchange membrane electrolyte. Electrochem. Commun. 2012, 16, 65-68.

9. Poynton, S. D.; Slade, R. C. T.; Omasta, T. J.; Mustain W. E.; Escudero-Cid, R.; Ocon, P.; Varcoe, J. R., Preparation of radiation-grafted powders for use as anion exchange ionomers in alkaline polymer electrolyte fuel cells. J. Mater. Chem. A. 2014, 2, 5124-5130.

10. Rao, V.; Hariyanto. C. C.; Stimming, U., Investigation of the ethanol electro-oxidation in alkaline membrane electrode assembly by differential electrochemical mass spectrometry. Fuel Cells. 2007, 7, 417-423.

11. Shao, M. H.; Adzic, R. R., Electrooxidation of ethanol on a Pt electrode in acid solutions: in situ ATR-SEIRAS study. Electrochim. Acta. 2005, 50 (12), 2415-2422.

12. Leung, L. W. H.; Chang, S.-C.; Weaver, M. J., J. Electroanal. Chem. & Interfacial Electrochem. 1989, 266 (2), 317-366.

13. Colmati, F.; Tremiliosi-Filho, G.; Gonzalez, E. R.; Berna, A.; Herrero, E.; Feliu, J. M., Surface structure effects on the electrochemical oxidation of ethanol on platinum single rystal electrodes. Faraday Discuss. 2008, 140, 379−397.

14. Camara, G. A.; Iwasita, T., Parallel pathways of ethanol oxidation: The effect if ethanol concentration. J. Electroanal. Chem. 2005, 578 (2), 315-321.

15. Heinen, M.; Jusys, Z.; Behm, R. J., Ethanol,, acetaldehyde and acetic acid adsorption .electrooxidation on a Pt thin film electrode under continuous electrolyte flow: An in situ ATR FTIRS flow cell study. J. Phys. Chem. C. 2010, 114 (21), 9850-9864.

16. Xia, X. H.; Liess, H. D. and Iwasita, T., Early stages in the oxidation of ethanol at low index single crystal platinum electrodes. J. Electroanal. Chem. 1997, 437 (1-2), 233-240.

17. Dutta, A. and Datta, J., Significant role of surface activation on Pd enriched Pt nano catalysts in promoting the electrode kinetics of ethanol oxidation: Temperature effect, product analysis & theoretical omputations. Int. J. Hyd. En. 2013, 38, 7789-7800.

18. Jiang, L.; Hsu, A.; Chu, D.; Chen, R., Ethanol electro-oxidation n Pt/C and PtSn/C catalysts in alkaline and acid solutions. Int. J. Hyd. En. 2010, 35, 365-372.

19. Schmidt, T. J.; Ross, P. N.; Markovic, N. M., Temperature-dependent surface electrochemistry on Pt single crystals alkaline electrolyte: Part 1: O oxidation. J. Phys. Chem. B. 2001, 105, 12082-12086.

20. López-Atalaya, M.; Moralloń , E.; Cases, F.; Vaźquez, J. L.; Peŕez, J. M., Electrochemical oxidation of ethanol on Pt(hkl) basal surfaces in NaOH and Na_2CO_3 media. J. Power Sources. 1994, 52 (1), 109-117.

21. Ma, L.; Chu, D. and Chen, R., Comparison of ethanol electrooxidation on Pt/C and Pd/C catalysts alkaline media. Int. J. Hyd. En. 2012, 37, 11185-11194.

22. Caram, J. A.; Gutiérrez, C., Study by cyclic voltammetry and potential-modulated reflectance spectroscopy of the electroadsorption of methanol and ethanol on a rhodium electrode in acid and alkaline media. J. Electroanal. Chem. 1992, 323, 213-230.

23. Freitas, R. G.; Pereira E. C.; Christensen, P. A., The selective oxidation of ethanol to CO_2 at $Pt_{pc}Ir$/Pt metallic multilayer nanostructured electrodes. Electrochem. Comm. 2011, 13, 1147-1150.

24. Freitas, R. G.; Antunes, E. P.; Christensen, P. A.; Pereira, E. C., The influence of Ir and Pt1Ir1 structure in metallic multilayers nanoarchitectured electrodes towards ethylene glycol electro-oxidation. J. Power Sources. 2012, 214, 351-357.

25. Christensen, P. A.; Jones, S. W. M. and Hamnett, A., In situ FTIR studies of ethanol oxidation at polycrystalline Pt in alkaline solution. J. Phys. Chem. C. 2012, 116, 24681−24689.

26. Russell, A. E.; Blackwood, D.; Anderson, M. R.; Pons, S. J., SNIFTIRS study of the behavior of the spectrum of carbon monoxide adsorbed on a platinum electrode in alcoholic solvents. Electroanal. Chem. 1991, 304 (1-2), 219-231.

27. Christensen, P. A.; Hamnett, A., In Comprehensive Chemical Kinetics. New Techniques for the Study of Electrodes and their Reactions, 1st ed.; Compton, R. G., Hamnett, A., Eds.; Elsevier: Amsterdam, 1989, Vol. 29, p 1.

28. Chen, Q. S.; Sun, S. G.; Zhou, Z. Y.; Chen, Y. X.; Deng, S. B., CoPt nanoparticles and their catalytic properties in electrooxidation of CO and CH_3OH studies by in-situ FTIRS. Phys. Chem. Chem. Phys. 2008, 10, 3645-3654.

29. Lin, W. F.; Christensen, P. A.; Hamnett, A.; Zei, M. S.; Ertl, G., The electro-oxidation of CO at the Ru(00001) single-crystal electrode surface. J. Phys. Chem. B. 2000, 104, 6642-6652.

30. Lin, W. F.; Christensen, P. A.; Hamnett, A., In situ FTIR studies on the effect of temperature on the adsorption and electrooxidation of CO at the Ru(0001) electrode surface. J. Phys. Chem. B. 2000, 104, 12002-12011.

31. Christensen, P. A.; Linares-Moya, D., The role of adsorbed formate and oxygen in the oxidation of methanol at a polycrystalline Pt electrode in 0.1 M KOH: An in situ Fourier transform infrared study. J. Phys. Chem. C. 2009, 114 (2), 1094-1101.

32. Christensen, P. A.; Hamnett, A.; Linares-Moya, D., The electro-oxidation of formate ions at a polycrystalline Pt electrode in alkaline solution: An in situ FTIR study. Phys. Chem. Chem. Phys. 2011, 13(24), 11739-11747.

33. Wurtz, C. A., Bulletin de la Société Chimique de France. 1872, 17, p436.

34. Griffiths, P. R. and de Haseth J. A., Fourier Transform Infrared Spectrometry. Wiley-Interscience: New York, 1986, 39-41.

35. Christensen, P. A. and Hamnett, A., "Techniques and Mechanisms in Electrochemistry", Chapman and Hall: London, 1994, 228-262

36. Lai, S. C. S.; Koper, M. T. M., Ethanol electro-oxidation on platinum in alkaline media. Phys. Chem. Chem. Phys. 2009, 11, 10446-10456.

37. Zhou, Z.-Y.; Wang, Q.; Lin, J.-L.; Tian, N.; Sun, S.G., In situ FTIR spectroscopic studies of electrooxidtion of ethanol on Pd electrode in alkaline media. Electrochim Acta. 2010, 55 (27), 7995-7999.

38. Fang, X.; Wang, L.; Shen, P. K.; Cui, G.; Bianchini, C., An in situ Fourier transform infrared spectroelectrochemical study on ethanol electrooxidation on Pd in alkaline solution. J. Power Sources. 2010, 195 (5), 1375-1378.

39. Christensen, P. A.; Hamnett, A., The oxidation of ethylene-glycol at a platinum-electrode in acid and base – An in situ FTIR study. J. Electroanal. Chem. 1989, 260, 347-359.

40. Śmiechowski, M.; Stangret, J., Molecular picture of hydroxide anion hydration in aqueous solutions studied by FT-IR ATR spectroscopy. J. Mol. Struct. 2007, 834-836, 239-248

41. Dreesen, L.; Humbert, C.; Hollander, P.; Mani, A. A.; Ataka, K.; Thiry, P. A.; Peremans, A., Study of the water/poly(ethylene glycol) interface by IR-visible sum-frequency generation spectroscopy. Chemical Physics Letters. 2001, 333, 327-331.

42. Berná, A.; Delgado, J. M.; Orts, J. M.; Rodes, A.; Feliu, J. M., Spectroelectrochemicall study of the adsorption of acetate anions at gold single crystal and thin-film electrodes. Electrochimica Acta, 2008. 53, 2309-2321.

43. CRC Handbook of Chemistry and Physics, D. R. Lide, Ed; CRC Press: Boca Raton, 1993-1994; 74, 8-47.

44. Brescia, F.; LaMer, V. K; Nachod, F. C., The temperature dependence of the dissociation constant of deuteroacetic acid. J. Am. Chem. Soc. 1940, 62, 614-617.

45. Wandlowski, T.; Ataka, K.; Pronkin, S.; Diesing, D., Surface enhanced infrared spectroscopy – Au(111-20nm)/sulphuric acid – New aspects and challenges. Electrochim. Acta. 2004, 49, 1233-1247.

46. Wang, H.; Jusys, Z.; Behm, R. J., Ethanol electrooxidation on a carbon-supported Pt catalyst: Reaction kinetics and product yields. J. Phys. Chem. C. 2004, 108, 19413-19424.

Figure captions

1. CVs of the 1 cm^2 Pt foil working electrode collected in 0.1M KOH, in the absence of ethanol, at 25 (—) and 50°C (—). Scan rate 100 mVs^{-1}.

2. CVs of the Pt foil working electrode collected in 0.1M KOH + 1 M EtOH at 25 (—) and 50°C (—). Scan rate of 100 mVs^{-1}.

3. Spectra (8 cm^{-1} resolution, 100 scans, 47 s per scan set) collected during the electro-oxidation of 1M ethanol in 0.1M KOH at 50°C, normalised to the reference spectrum collected at -0.85V.

4. Spectra collected during the experiment depicted in fig. 3 at the transition potential of -0.4 V, and during the experiment at 25ºC at the transition potential of -0.1 V.

5. (a) Plots of the intensities of the features in figs. 3 and 4 vs potential; (b) the intensities of the bands in (a) normalised to their maximum values.

6. Spectra collected at -0.6 V vs. MMO during the ethanol oxidation experiments carried out in fig. 4 at 25ºC and 50ºC.

7. The spectra collected above -0.3 V, normalised to that collected at -0.3 V, during the experiment depicted in fig. 3 over the range from (a) 4000-1050 cm^{-1} and (b) below 2000 cm^{-1}.

8. In-situ FTIR spectra collected at 0.4 V during the experiments carried out at 25 and 50 °C, normalised to the spectra collected at -0.1 V (25 °C) and -0.3 V (50 °C). See text for details.

9. In-Situ FTIR spectra collected at 0.4V during experiments analogous to those depicted in fig. 3, normalised to spectra collected at -0.85V and in the absence of 1 M EtOH.

10. In-Situ FTIR spectra collected at 0.4V during the experiments depicted in figs. 8 and normalised to the spectra taken at -0.1V (25 ºC) or -0.4V (50 ºC) over the spectral range 2050 – 1050 $cm^{-.1}$.

11. Plots of the intensities of the various features in figs. 7(a) and (b) as a function of potential.

Graphic for table of contents

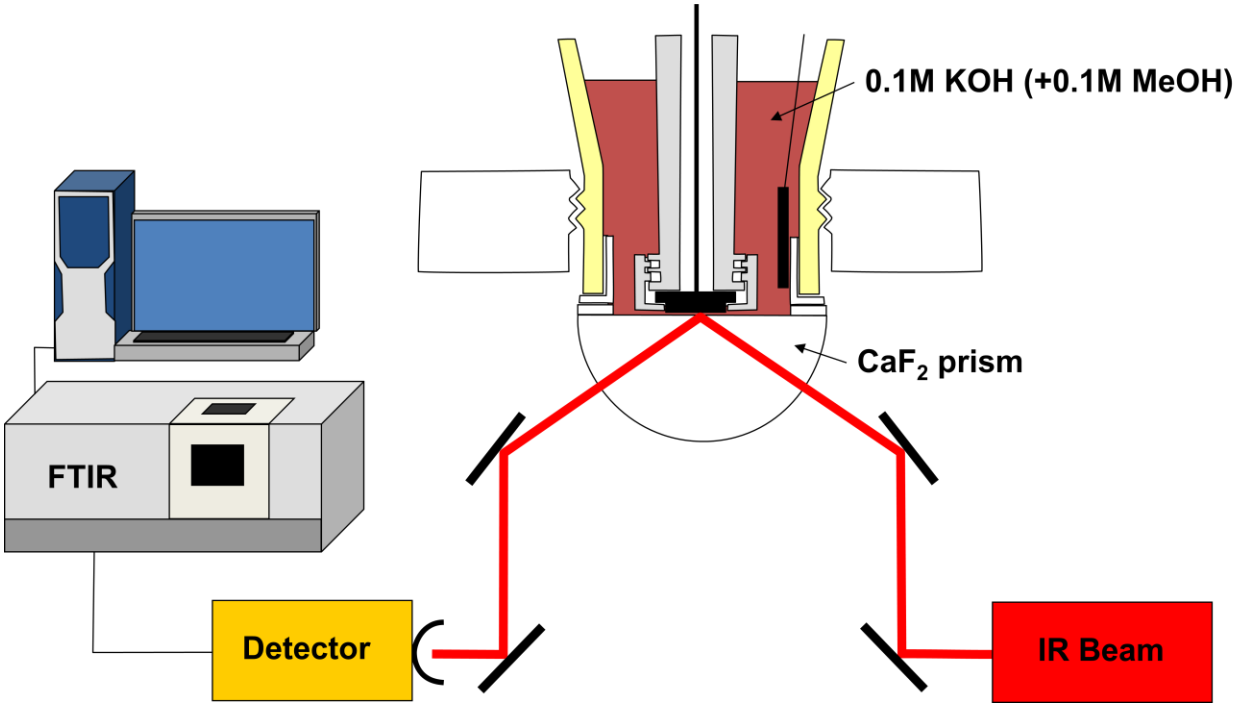

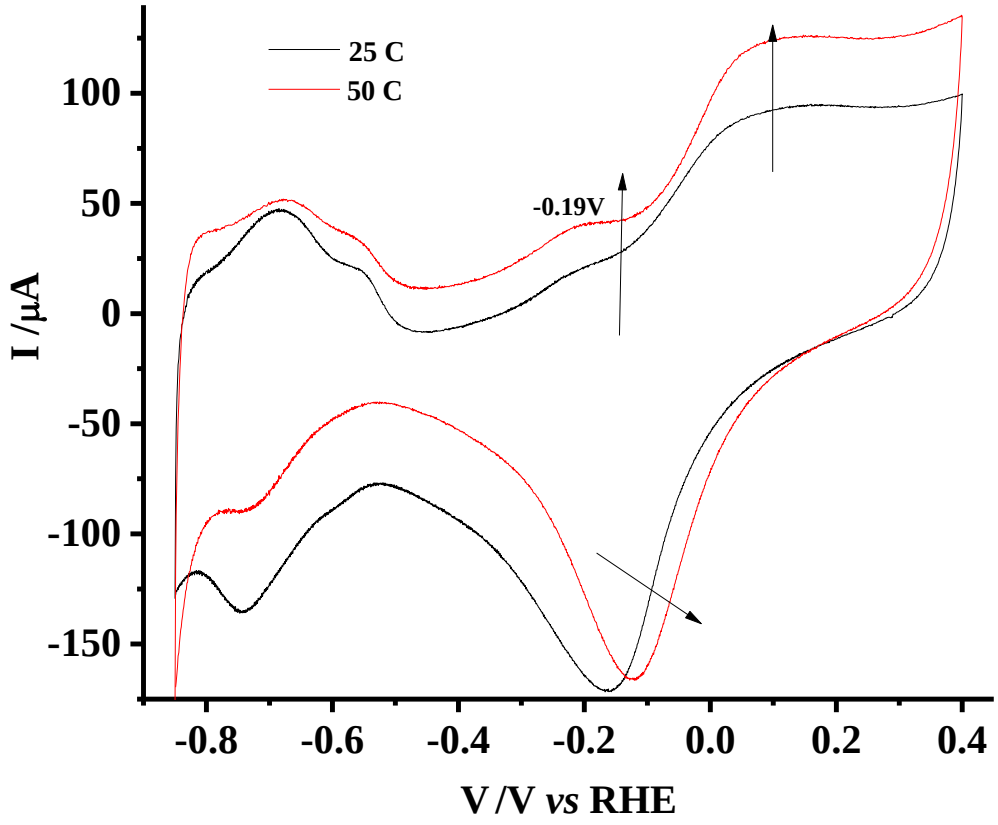

Figure 1

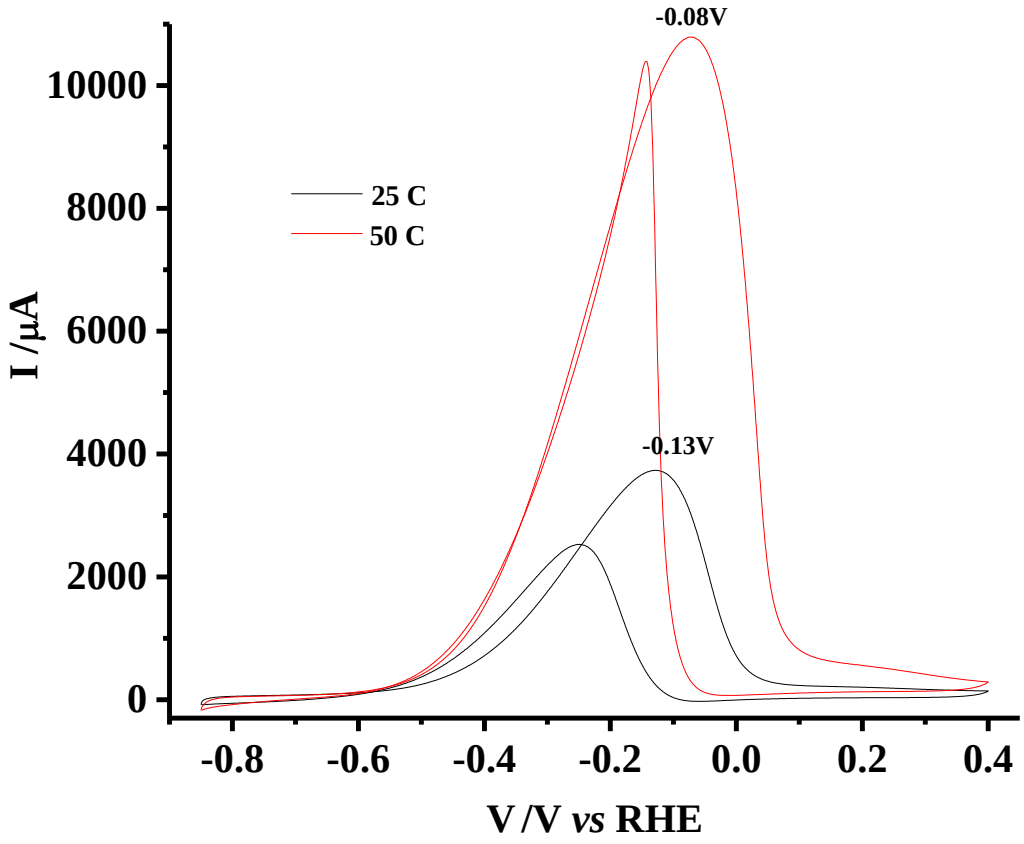
-0.08V
10000
8000
6000
4000
2000
0
25 C
50 C
I /μA
-0.13V
-0.8
-0.6
-0.4
-0.2
0.0
0.2
0.4
V /V vs RHE

Figure 2

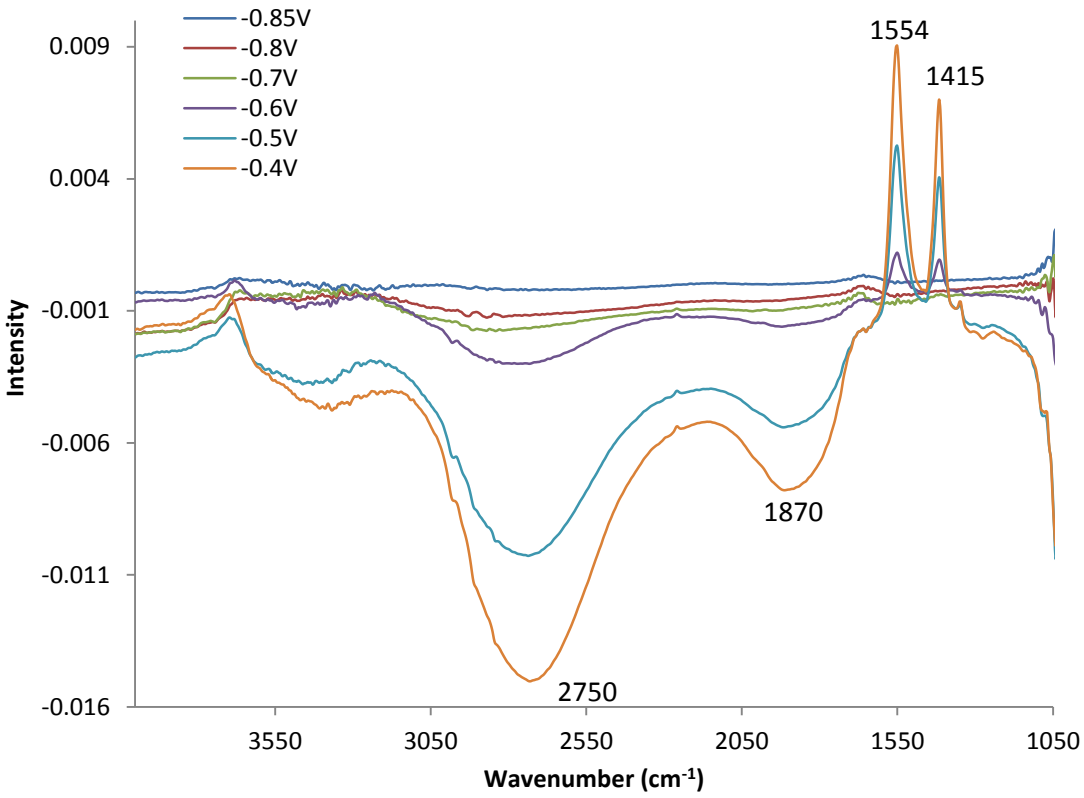

Figure 3

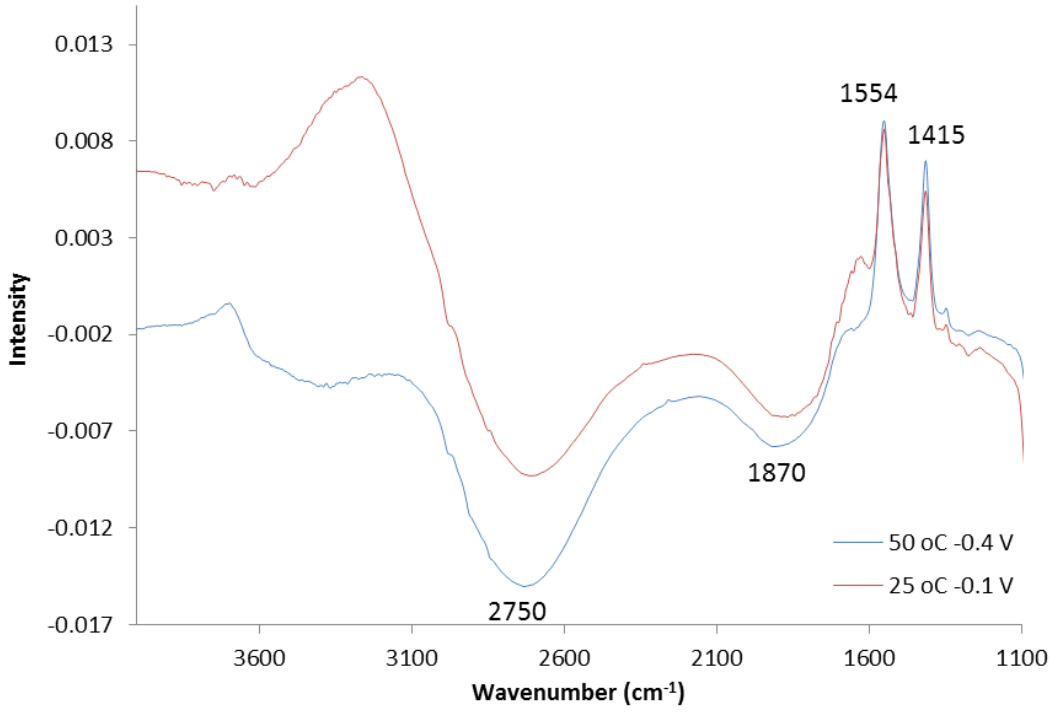

Figure 4

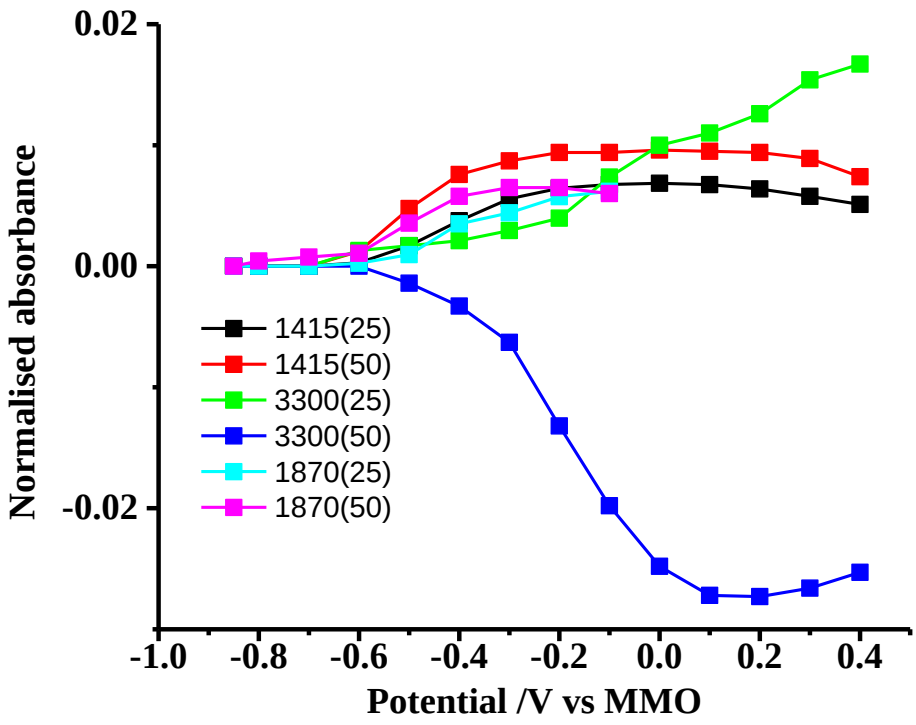
0.02
0.00
-0.02
Normalised absorbance
1415(25)
1415(50)
3300(25)
3300(50)
1870(25)
1870(50)
-1.0
-0.8
-0.6
-0.4
-0.2
0.0
0.2
0.4
Potential /V vs MMO

(a)

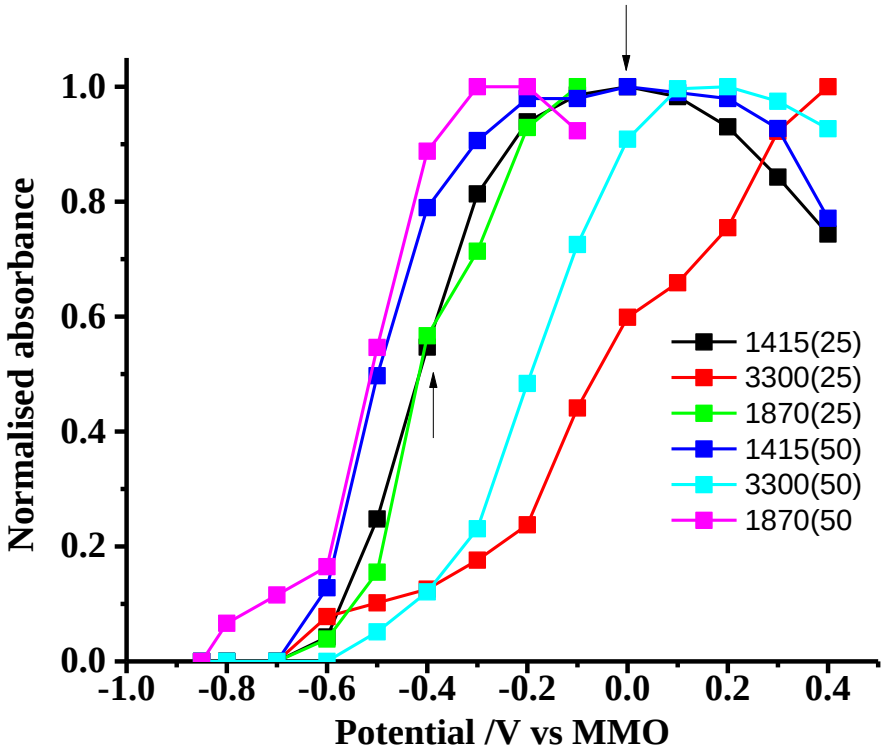
Normalised absorbance
1.0
0.8
0.6
0.4
0.2
0.0
-1.0
-0.8
-0.6
-0.4
-0.2
0.0
0.2
0.4
Potential /V vs MMO
1415(25)
3300(25)
1870(25)
1415(50)
3300(50)
1870(50

(b)

Figure 5

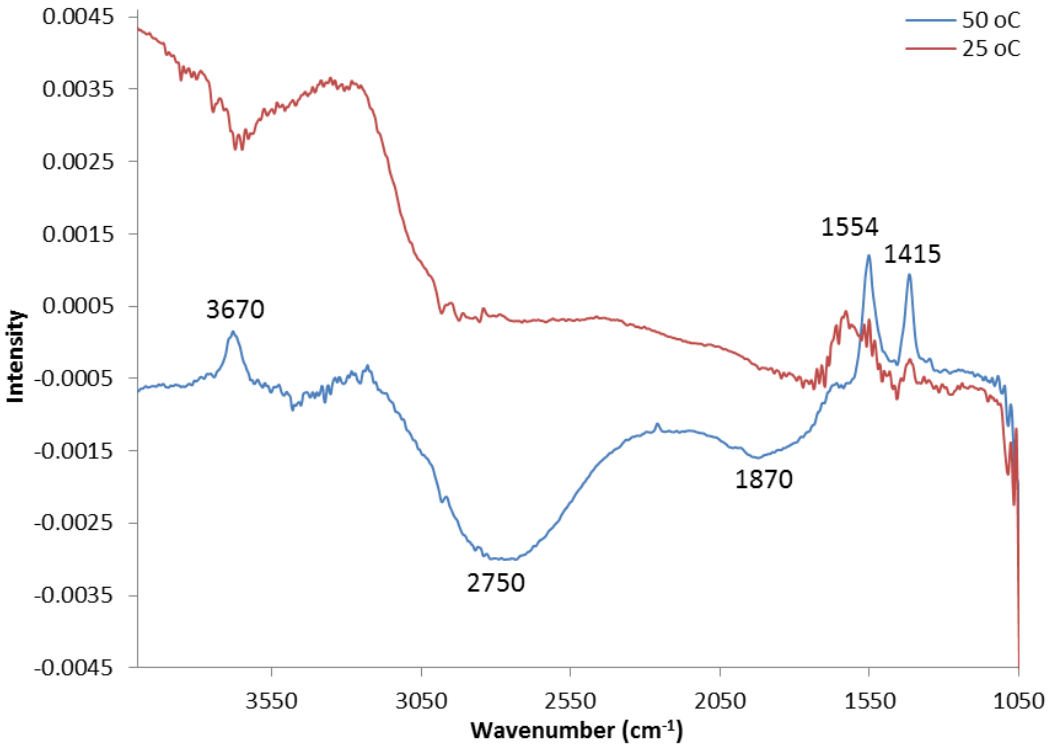
0.0045
0.0035
0.0025
0.0015
0.0005
-0.0005
-0.0015
-0.0025
-0.0035
-0.0045
Intensity
3550
3050
2550
2050
1550
1050
Wavenumber (cm-1)
50 oC
25 oC
3670
2750
1870
1554
1415

Figure 6

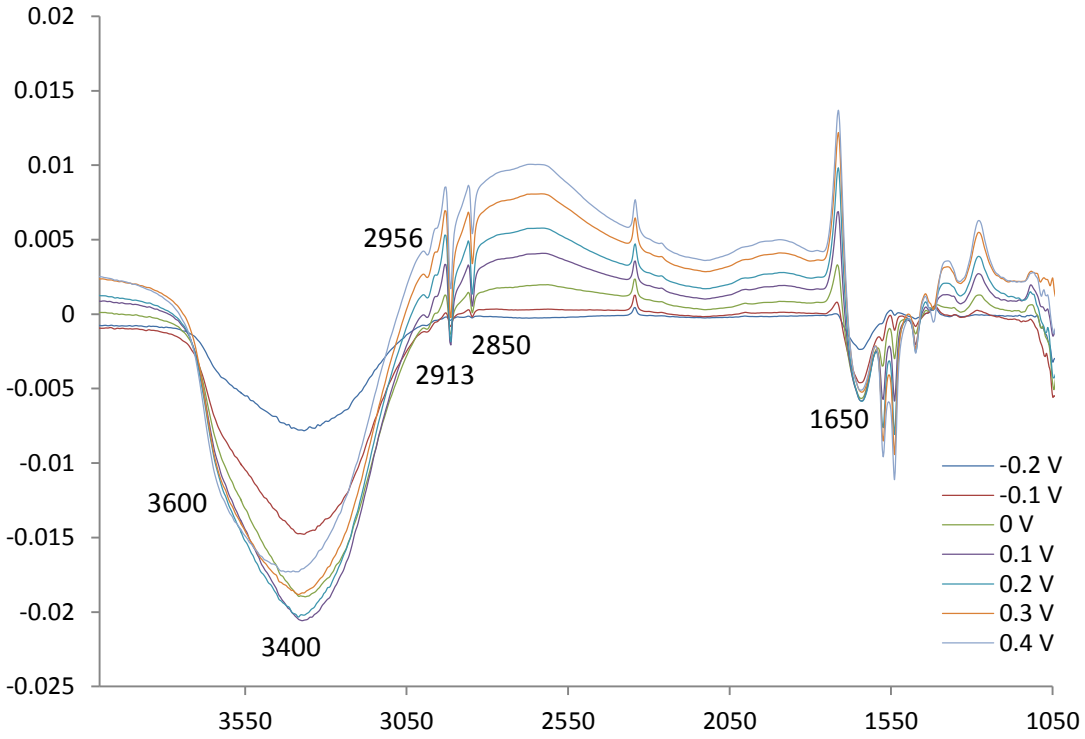
0.02
0.015
0.01
0.005
0
-0.005
-0.01
-0.015
-0.02
-0.025
3550
3050
2550
2050
1550
1050
2956
2850
2913
1650
3600
3400
-0.2 V
-0.1 V
0 V
0.1 V
0.2 V
0.3 V
0.4 V

(a)

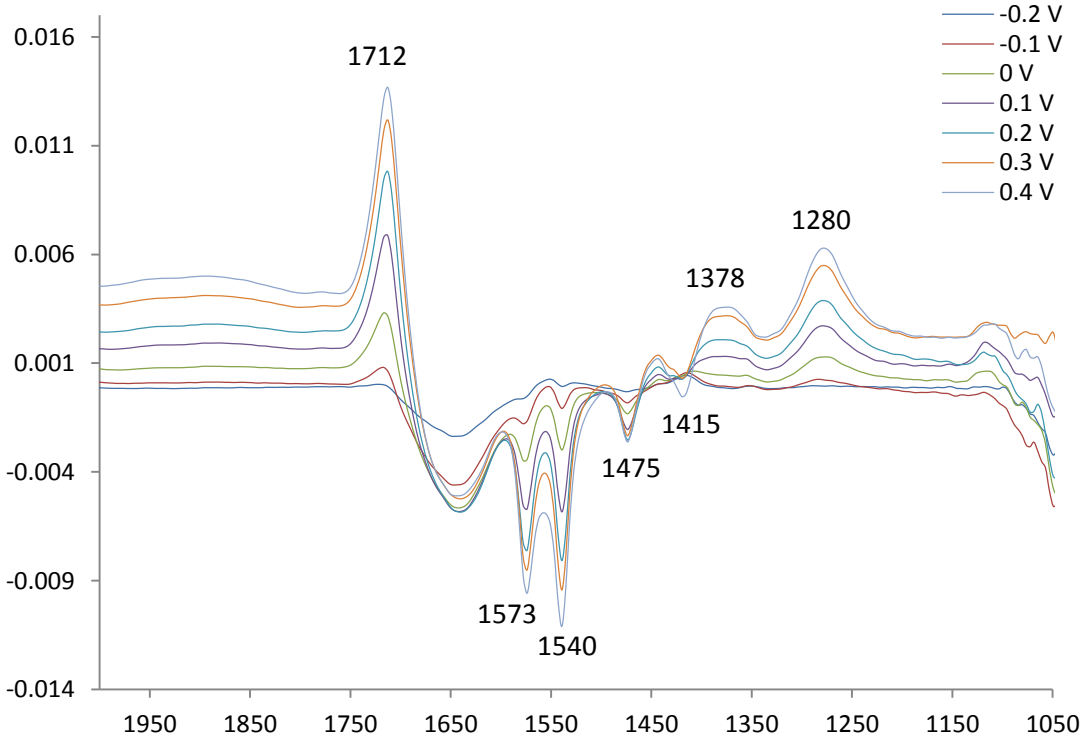
0.016
0.011
0.006
0.001
-0.004
-0.009
-0.014
1950
1850
1750
1650
1550
1450
1350
1250
1150
1050
1712
1280
1378
1415
1475
1573
1540
-0.2 V
-0.1 V
0 V
0.1 V
0.2 V
0.3 V
0.4 V

(b)

Figure 7

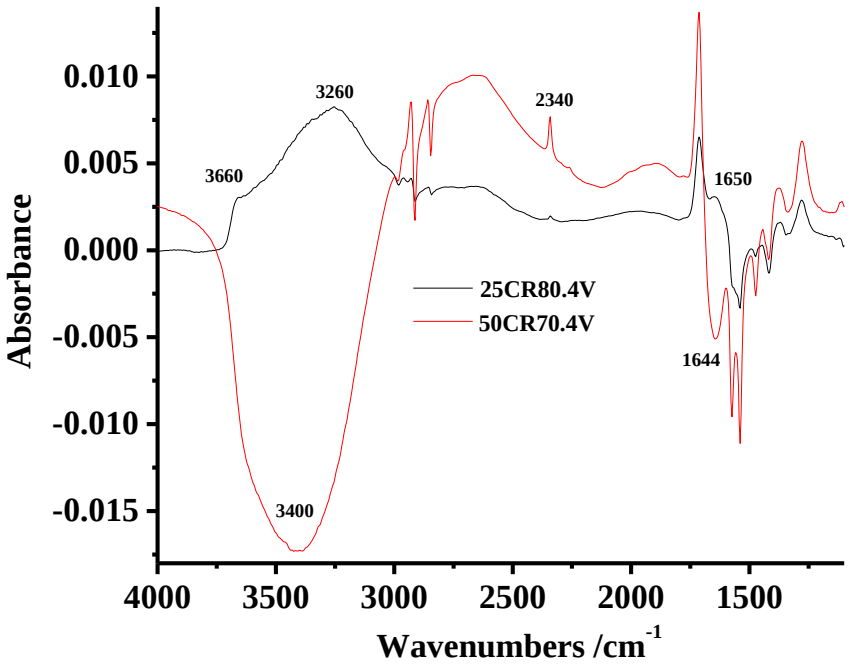

Figure 8.

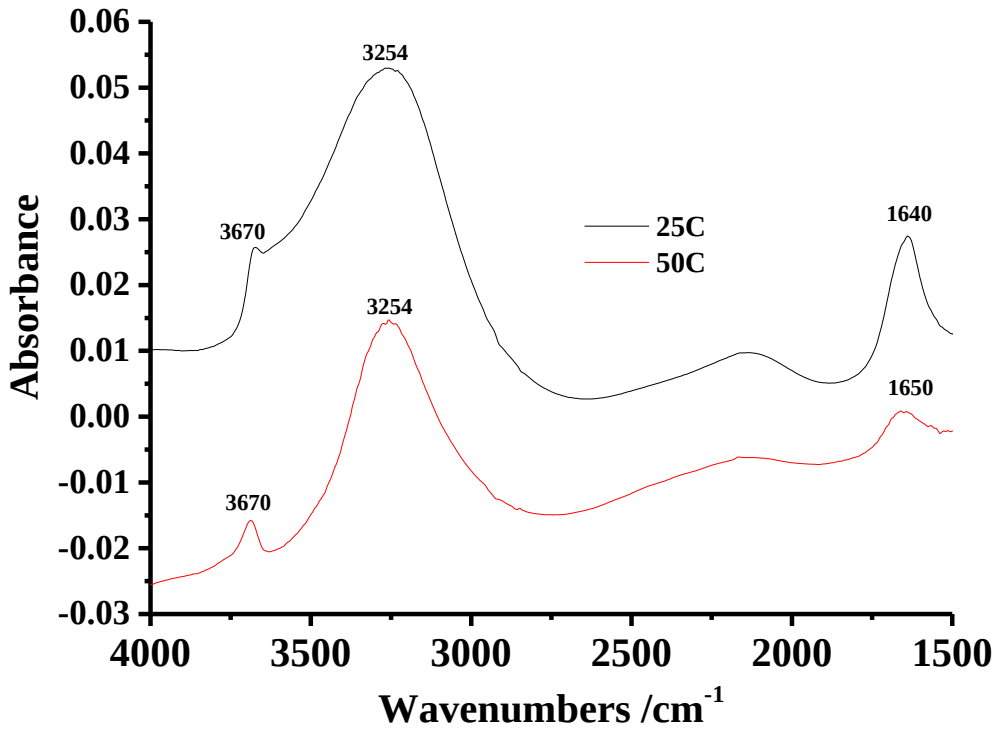
0.06
0.05
0.04
0.03
0.02
0.01
0.00
-0.01
-0.02
-0.03
Absorbance
3254
3670
25C
50C
1640
3254
1650
3670
4000
3500
3000
2500
2000
1500
Wavenumbers /cm-1

Figure 9

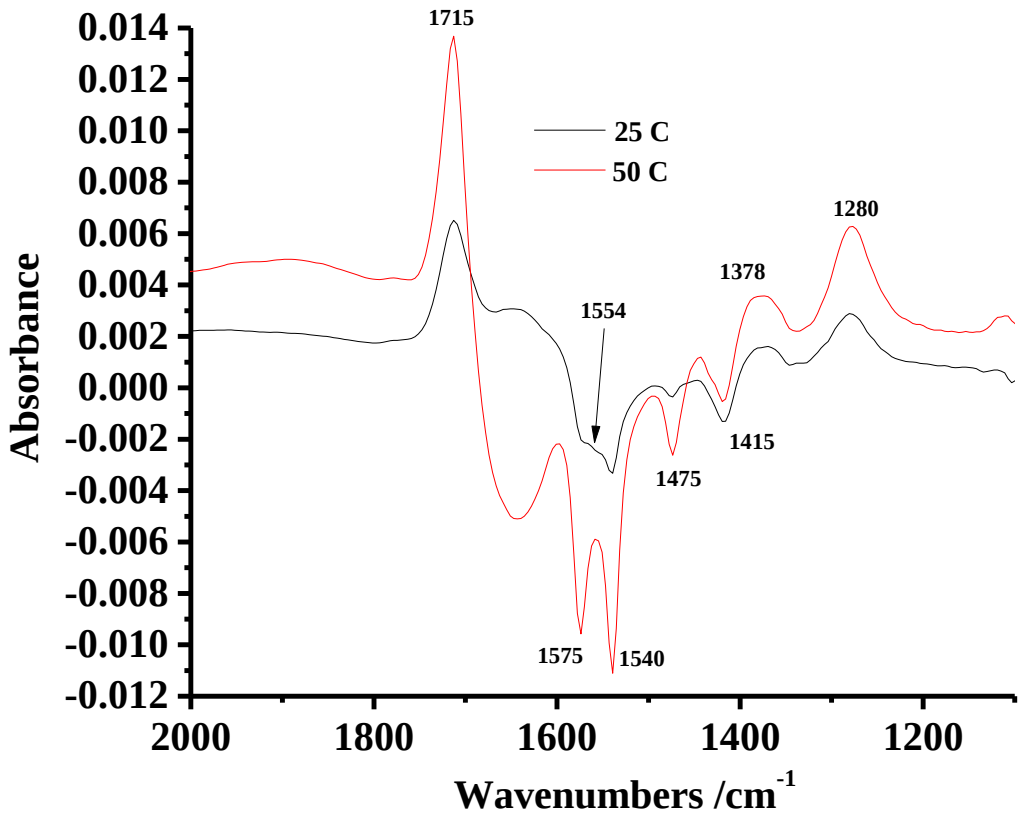
0.014
0.012
0.010
0.008
0.006
0.004
0.002
0.000
-0.002
-0.004
-0.006
-0.008
-0.010
-0.012
Absorbance
2000
1800
1600
1400
1200
Wavenumbers /cm-1
25 C
50 C
1715
1554
1378
1280
1415
1475
1575
1540

Figure 10

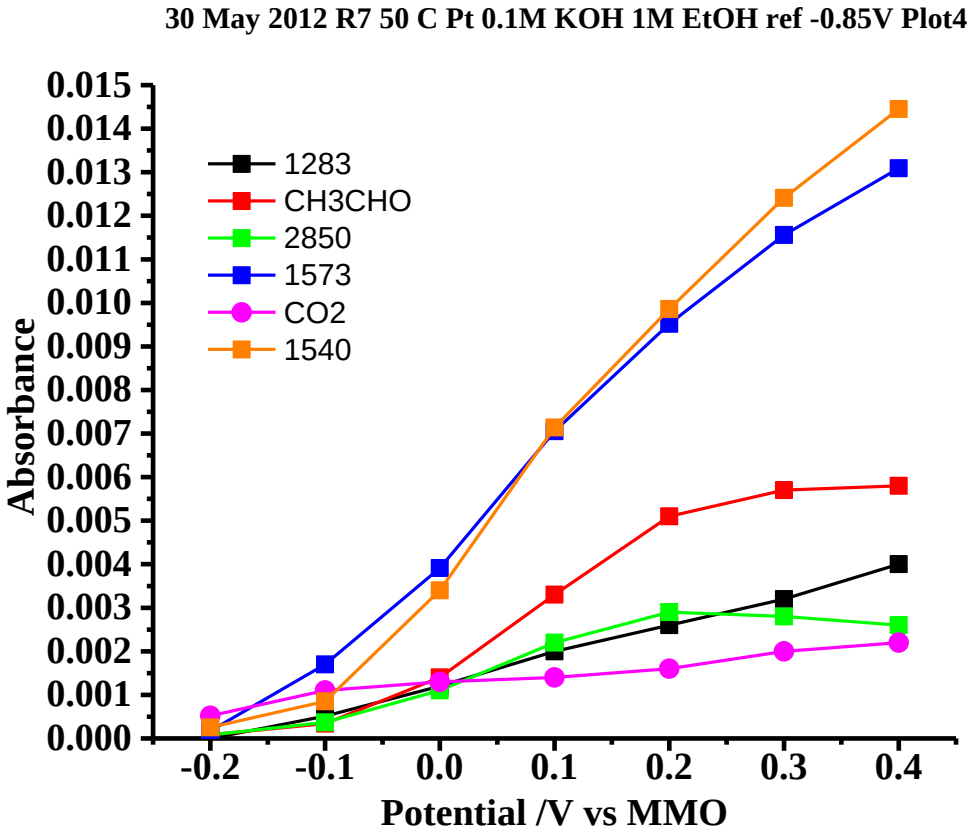
30 May 2012 R7 50 C Pt 0.1M KOH 1M EtOH ref -0.85V Plot4
Absorbance
Potential /V vs MMO
1283
CH3CHO
2850
1573
CO2
1540
0.015
0.014
0.013
0.012
0.011
0.010
0.009
0.008
0.007
0.006
0.005
0.004
0.003
0.002
0.001
0.000
-0.2
-0.1
0.0
0.1
0.2
0.3
0.4

Figure 11